10-1-2011

Localized Recrystallization in Cast Al-Si-Mg Alloy During Solution Heat Treatment: Dilatometric and Calorimetric Studies

S. K. Chaudhury

V. Warke

S. Shankar

Diran Apelian
Worcester Polytechnic Institute, dapelian@wpi.edu

Localized Recrystallization in Cast Al-Si-Mg Alloy during Solution Heat Treatment: Dilatometric and Calorimetric Studies

S.K. CHAUDHURY, V. WARKE, S. SHANKAR, and D. APELIAN

During heat treatment, the work piece experiences a range of heating rates depending upon the sizes and types of furnace. When the Al-Si-Mg cast alloy is heated to the solutionizing temperature, recrystallization takes place during the ramp-up stage. The effect of heating rate on recrystallization in the A356 (Al-Si-Mg) alloy was studied using dilatometric and calorimetric methods. Recrystallization in as-cast Al-Si alloys is a localized event and is confined to the elasto-plastic zone surrounding the eutectic Si phase; there is no evidence of recrystallization in the center of the primary Al dendritic region. The size of the elasto-plastic zone is of the same order of magnitude as the Si particles, and recrystallized grains are observed in the elasto-plastic region near the Si particles. The coefficient of thermal expansion of Al is an order of magnitude greater than Si, and thermal stresses are generated due to the thermal mismatch between the Al phase and Si particles providing the driving force for recrystallization. In contrast, recrystallization in Al wrought alloy (7075) occurs uniformly throughout the matrix, stored energy due to cold work being the driving force for recrystallization in wrought alloys. The activation energy for recrystallization in as-cast A356 alloy is 127 KJ/mole. At a slow heating rate of 4.3 K/min, creep occurs during the heating stage of solution heat treatment. However, creep does not occur in samples heated at higher heating rates, namely, 520, 130, and 17.3 K/min.

DOI: 10.1007/s11661-011-0716-x

I. INTRODUCTION

THE Al-Si-Mg alloys are widely used for automotive and aerospace applications owing to their good castability and high strength-to-weight ratio.[1–3] Normally, these alloys are solution heat treated, quenched, and subsequently aged to obtain a good combination of tensile strength and ductility.[4–7] In our previous studies, we reported the effect of heating rate on solutionizing and artificial aging characteristics of cast Al alloys.[8–10] The heating rate plays an important role in altering the phase transformation mechanism and kinetics during various heat-treatment stages. Several reports have been published on the effect of heating rate on phase transformation(s) during heat treatment of wrought Al alloys;[11–13] however, not much has been reported on the effect of heating rate in cast Al alloys.

One of the most common phenomena observed during annealing of wrought Al alloys is recrystallization of the strained Al matrix. Recrystallization results in the formation of strain-free grains.[14–17] The driving force for recrystallization in wrought alloys is the mechanical energy stored in the Al matrix due to cold working. Cold working increases the defect concentration in the matrix and, thereby, increases stored energy. These defects can be either point defects (vacancies or interstitial), line defects (dislocations), or planar defects (stacking faults). It is well known that recrystallization increases the ductility and decreases the strength of wrought alloys. However, the effect of recrystallization on mechanical properties in as-cast Al-Si alloys (which are not cold worked) has not been studied.

The effect of heating rate on the recrystallization behavior of as-cast A356 alloy during the heating stage of solution heat treatment was studied through dilatometry, calorimetry, and thermal analyses. Dilatometric test measures the coefficient of thermal expansion of the sample over a wide range of temperatures. The coefficient of thermal expansion is an important engineering property for many industrial applications pertinent to dimensional stability. Al alloys are subjected to thermal treatment comprised of hysteresis of temperature to tailor mechanical properties. During the ascent or descent of temperature, constituent phases in the alloy do not expand or contract uniformly. This may cause permanent deformation in the matrix. The published literature lacks data on the thermal expansion behavior in Al-Si-Mg alloys. The objective of this study is to carry out an in-depth analysis of data generated from dilatometric, calorimetric, and thermal analyses tests, and to provide a mechanistic understanding of the effect of heating rate on recrystallization in cast A356 alloys.

S.K. CHAUDHURY, Engineer, is with Honeywell Turbo Technologies, Torrance, CA 90505. V. WARKE, Engineer, is with the Bodycote Thermal Processing, Andover, MA 01810. S. SHANKAR, Orlick Chair Professor, is with Light Metal Casting Research Centre, McMaster University, Hamilton, ON L8S 4L7. D. APELIAN, Howmey Professor of Engineering, is with Worcester Polytechnic Institute, Metal Processing institute, Worcester, MA 01609. Contact e-mail: dapelian@wpi.edu

Manuscript submitted January 24, 2007.
Article published online June 15, 2011

II. EXPERIMENTAL PROCEDURE

A. *Alloy Preparation*

Dilatometry and calorimetry studies were conducted on A356 (Al-Si-Mg) alloy, whose chemical composition is shown in Table I. The alloy was modified with Al-9.9 wt pct Sr and grain refined with Al-5 wt pct Ti master alloy. The alloy was cast in a ferrous permanent mold, preheated to 673 K (400 °C). The pouring temperature was 1073 K (800 °C). Before casting, the melt was degassed using a rotary impeller by purging ultra-high-purity Ar gas through the melt for 45 minutes.

B. *Dilatometric Test*

Cylindrical samples with excellent surface finish for dilatometric tests were machined from cast Al-Si-Mg alloy using an electrical discharge machine. Dilatometric tests were conducted using an MMC quench dilatometer. Samples were heated to 813 K (540 °C) from room temperature at four different heating rates. These are 520, 130, 17.3, and 4.3 K/min. Thermocouples were welded on the specimen to record temperature. The change in length (ΔL) was measured during the heating and cooling stages. Dimensions of each sample were measured before and after the test using a screw gage. Average values of the coefficient of thermal expansion (α) of the A356 alloy heated at different rates were determined by regression analysis, where $\alpha = \frac{1}{l_o}\left(\frac{d\Delta L}{dT}\right)$ and l_o = original length. The phase transformation temperature (T) was determined by plotting the first derivative of the change in length (*i.e.*,$\frac{d\Delta L}{dT}$) *vs* T. The first derivative (*i.e.*,$\frac{d\Delta L}{dT}$) usually varies linearly with temperature for most alloys. Any deviation from this linearity on the $\frac{d\Delta L}{dT}$ *vs* T plot signifies a phase transformation.

C. *Differential Scanning Calorimetric Test*

The calorimetric study was conducted using a Perkin-Elmer DSC-7 calorimeter (PerkinElmer, Waltham, MA) on drill chips machined from the A356 alloy. Care was taken to avoid contamination during drilling operations. Tests were conducted at different heating rates. Sample heating rates were 4.3 and 17.3 K/min.

D. *Thermal Analysis*

Thermal analysis was carried out to study the phase transformation in as-cast A356 alloy (not machined) during the heating stage of solution heat treatment. A phase transformation is accompanied by a release (exothermic) or absorption (endothermic) of thermal energy, which is usually detected by superimposing the first derivative curve (dT/dt *vs* t) on the heating profile (T *vs* t). Temperature measurements were carried out using DASYLab software (DASYLab, Monchengladbach, Germany) coupled with a data acquisition system. A K-type thermocouple was used for this study. The thermocouple was placed at the center of the permanent mold cavity, and the melt was poured and allowed to solidify around the thermocouple. Subsequently, the sample was heated in a conventional electrical resistance furnace (CF) with slow heating rate (~18 K/min) and a fluidized bed (FB) furnace with a high heating rate (132 K/min).

Table I. Chemical Composition of A356 Alloy

Si	Mg	Fe	Ti	Sr	Al
7.00	0.35	0.12	0.15	0.02	balance

E. *Microstructural Characterization (Scanning Electron Microscopy and Transmission Electron Microscopy)*

Samples for scanning electron microscopy (SEM) were prepared by standard procedures of grinding using different grits of emery paper and electropolishing at 30 V for 20 seconds. The composition of the electrolyte (in volume percent) was 60 pct ethyl alcohol, 20 pct percholoric acid, and 20 pct ethylene glycol. Samples for transmission electron microscopy (TEM) were prepared by focused ion beam (FIB) milling. The procedure for preparing TEM foil using FIB is reported elsewhere.[18] The advantage of using FIB to prepare TEM foil is that large TEM samples can be prepared from an exact region of interest.

III. RESULTS AND DISCUSSION

Results of dilatometric analysis, differential scanning calorimetry (DSC) analysis, thermal analysis, and microstructural analysis are presented and discussed in the ensuing Sections III–A through III–D.

A. *Dilatometric Analysis*

1. *Dimensional stability*

Figure 1 shows the change in length of samples heated at different rates. The coefficient of thermal expansion was determined by linear regression of strain *vs* temperature data and is given in Table II for different heating rates. The linear regression shown in Figure 1 was carried out for temperature data ranging from room temperature to the temperature just below the

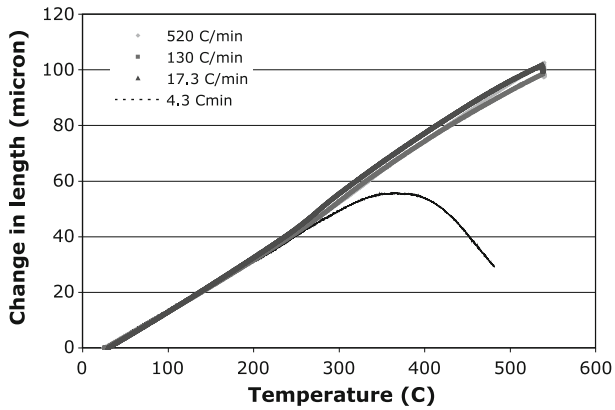

Fig. 1—Plot of change in length (ΔL) *vs* temperature.

Table II. Mean Values of Coefficient of Thermal Expansion (Prior to Transformation) and Dimensional Change of Samples after Dilatometry Test at Different Heating Rates

Heating Rate (K/min)	Initial Dimension		Final Dimension		Dimensional Change		Average Coefficient of Thermal Expansion $\times 10^{-5}$ (/K)	R^2 (Linear Regression Fit)
	L_0 (mm)	D_0 (mm)	L_f (mm)	D_f (mm)	ΔL (mm)	ΔD (mm)		
520	8.005	2.991	8.005	2.991	0	0	2.5334	0.9986
130	7.994	3.004	7.990	3.004	–0.004	0	2.5044	0.9987
17.3	7.985	2.9976	7.986	2.9976	0.001	0	2.6262	0.9987
4.3	7.9983	2.9993	7.9043	3.0163	–0.094	0.0637	2.2279	0.9996

recrystallization start temperature. Recrystallization start temperatures are 548, 508, 500, and 470 K (275, 235, 227, and 197 °C) at heating rates of 520, 130, 17.3, and 4.3 K/min, respectively. The thermal expansion depends on the heating rate. At a slow heating rate (4.3 K/min), the value of thermal expansion is lower as compared to high heating rates. No noticeable change of thermal expansion of A356 alloy is measured when the heating rate is varied to 17.3, 130, and 520 K/min.

Further, Table II shows that there is no significant change in sample dimensions before and after the dilatometric tests were conducted at high heating rates (*i.e.*, 17.3, 130, and 520 K/min), whereas for the low heating rate value (4.3 K/min), the dimensional change (both length and diameter) was significant. The variation of strain with temperature is almost reproducible during heating and cooling except in the case of the lowest heating rate (4.3 K/min), where a significant decrease in strain is noticed during the temperature ramp-up stage. This is because creep occurred when the sample was heated at the lowest heating rate, thus resulting in permanent deformation of the test piece. Results of the dilatometric test show that heating the test piece at the slowest heating rate (4.3 K/min) adversely affects the dimensional stability of A356 alloy casting.

2. *Recrystallization*

Dilatometry results (Figures 2 and 3) show that the as-cast A356 (Al-Si-Mg) alloy undergoes recrystallization, though the cast alloy was not cold worked. This is evident from the plot of dL/dT *vs* T (Figure 2) at different heating rates. In general, a typical metallic trend yields a constant value of dL/dT value in a certain temperature range. A phase transformation is marked by a change in the value of dL/dT at the transformation temperature. Table III presents the variation of the recrystallization temperature with heating rates. It is noted that the recrystallization start temperature decreases with decreasing heating rate.

Table III also presents an interesting observation. One of the samples was treated to two thermal cycles: (1) heated at 130 K/min to 813 K (540 °C), isothermally held for 5 minutes at 813 K (540 °C), and cooled rapidly at 30 K/min; and (2) reheated at 130 K/min to 813 K (540 °C), isothermally held for 30 minutes at 813 K (540 °C), and cooled rapidly at 30 K/min. Recrystallization is observed during the heating stage in both thermal cycles, as presented in Table III (4 and 4-R min ramp-up time). The reoccurrence of recrystallization during reheating of the sample is due to the *in-situ* nature of the driving force for recrystallization, *i.e.*, generation of thermal stresses owing to mismatch at the

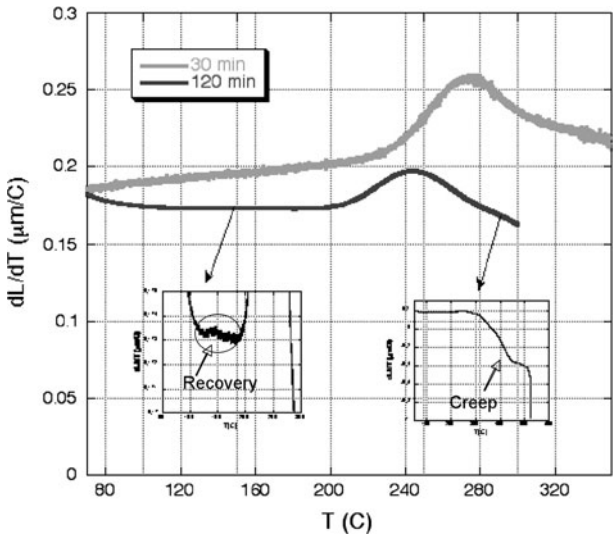

Fig. 2—Typical dilatometry plots of A356 alloy during temperature ramp-up stage. Samples were heated to 813 K (540 °C) at 4.3 and 17.3 K/min heating rates.

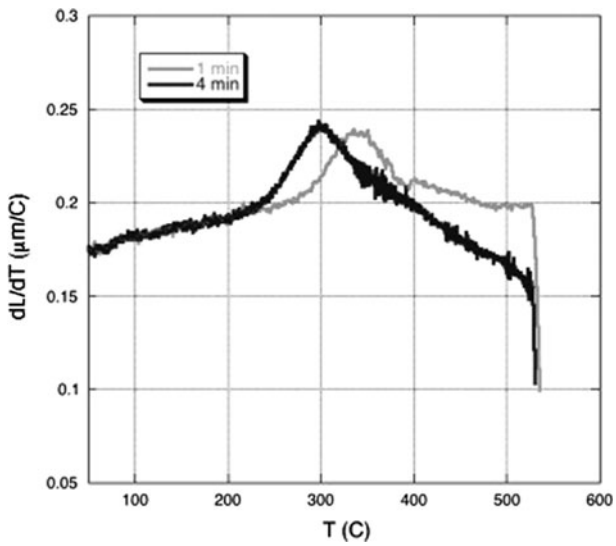

Fig. 3—Typical dilatometry plots of A356 alloy during temperature ramp-up stage. Samples were heated to 813 K (540 °C) at 130 and 520 K/min heating rates.

Table III. Recrystallization Data Determined by Dilatometric and DSC Tests

Ramp Time (min)	Heating Rate (K/min)	Recrystallization Start Temperature [K (°C)]		Recrystallization End Temperature [K (°C)]		Activation Energy (kJ/mol)*
		Dilatometry	DSC	Dilatometry	DSC	
1	520	548 (275)	—	613 (340)	—	127
4	130	508 (235)	—	572 (299)	—	
4-R**	130	528 (255)	—	608 (335)	—	
30	17.3	500 (227)	434 (161)	547 (274)	490 (217)	
120	4.3	470 (197)	416 (143)	516 (243)	465 (192)	

*From dilatometric test.
**Reheated sample (sample reheated at 130 K/min (*i.e.*, second thermal cycle)).

interfaces between Al and Si phases during cooling and heating stages. In addition, there is a delay in the onset of recrystallization in the reheated sample (4-R min ramp-up time) as compared to those when the sample was heated during the first cycle (4 min ramp-up time). This is because the recrystallization rate is high when the grain size is small. The observed delay in the recrystallization process in the reheated sample is due to the difference in the initial grain structure between the first and second heating cycles. The grain size of the eutectic Al phase during the first heating cycle was smaller than that during the second heating cycle.

The activation energy was calculated using the modified Kissinger model,[19,20] which is represented by Eq. [1]:

$$\ln\left(\frac{T_f^2}{Q}\right) = \frac{E}{RT_f} + \ln\left(\frac{E}{RK_o}\right) + \ln\left(b_f^*\right) \qquad [1]$$

Here, T_f = transformation start temperature, Q = heating rate, E = activation energy, and K_o and b_f^* are constants. The activation energy calculated by regression analysis is 127 KJ/mol.

In addition to the recrystallization peak, recovery is also observed in the case of the slowest heating rate (*i.e.*, 4.3 K/min). However, no recovery peaks are noted for higher heating rates (520, 130, and 17.3 K/min). This is because sufficient time for recovery was not available at higher heating rates.

3. *Creep during heat treatment*

It is evident from the dilatometry plot shown in Figure 1 that creep occurred only when the sample was heated at the low heating rate of 4.3 K/min. At the low heating rate of 4.3 K/min, creep started at 623 K (350 °C), which is far below the solidus temperature. Hence, the possibility of incipient melting is ruled out. The stress applied during the dilatometry test was 0.14 MPa, which is low. Hence, it is very unlikely that the mechanism of creep is by dislocation climb. Hence, despite the generation of dislocations during rapid heating (as discussed later in Section B on TEM analysis) no creep was observed when the sample was heated at rates higher than 4.3 K/min. The mechanism of creep in cast Al-Si-Mg alloy heated at 4.3 K/min is due to either bulk or grain boundary diffusion. The bulk diffusion is due to vacancy or interstitial diffusion (Nabarro–Herring creep). However, creep due to grain boundary diffusion is not ruled out, since no TEM observations were made on grain boundaries. In general, grain boundary diffusion is favored at relatively low temperatures, as it requires less activation energy, whereas bulk diffusion is favored at high temperatures. For bulk diffusion, atoms diffuse through vacancies or interstitial sites. Since bulk diffusion is a relatively slow process, creep occurred only in the samples tested at the slow heating rate of 4.3 K/min. The important finding of this study is that creep can take place during solution heat treatment of cast Al alloys at slow heating rates in spite of the fact that there is no externally applied stress. In industrial heat treating practices, castings are stacked over each other and the resultant stress induced by the weight of castings on each other may be sufficient to result in creep. Therefore, to avoid such deformation, care should be taken to heat the casting at a very fast rate and reduce the overall solution heat-treatment time to less than an hour. In order to observe the effect of high heating rate and holding time, a retest was conducted on the sample (heated at 130 K/min), where the sample was reheated at 130 K/min and isothermally held at 813 K (540 °C) for 30 minutes. No creep was observed, as shown in Figure 4. Thus, we infer that rapid heating and reduced holding time can avoid creep during heat treatment of cast Al alloys.

B. *Differential Scanning Calorimetric Analysis*

A typical DSC thermograph of A356 alloy during the temperature ramp-up stage of solution heat treatment is shown in Figure 5. The DSC result is consistent with the dilatometric test. An exothermic peak due to recrystallization was observed at different heating rates. The recrystallization start temperature decreases with a decrease in heating rate. The recrystallization temperature at different heating rates determined *via* DSC is lower as compared to those determined by dilatometry tests (Table III). The difference between recrystallization temperature determined from DSC and dilatometry tests could be due to differences in the sensitivity of measuring methods. Enthalpies for transformation at 17.2 and 4.3 K/min are 8.469 and 9.446 J/g, respectively.

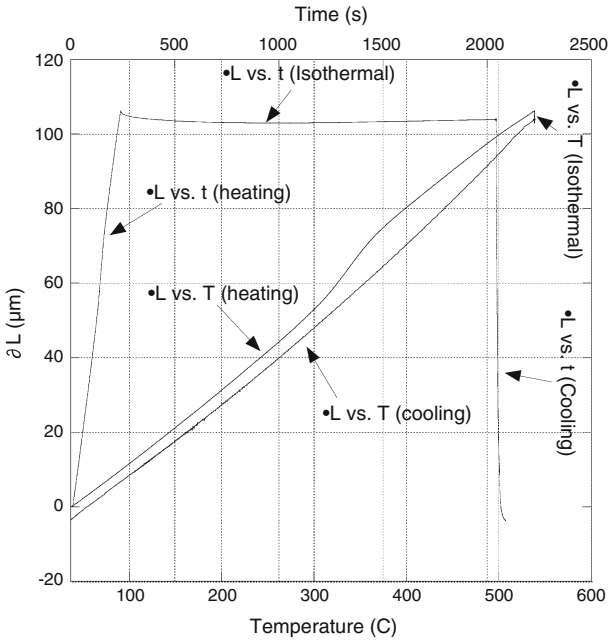

Fig. 4—Plot of change in length (∂L) *vs* temperature and strain *vs* time of sample reheated to 813 K (540 °C) at 130 K/min.

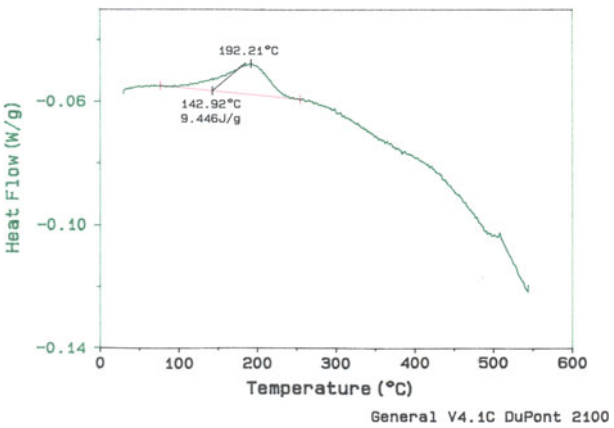

Fig. 5—DSC plot of Al-Si-Mg alloy drilled chips during the heating stage of solution heat treatment in CF (heating rate = 4.3 K/min).

C. *Anomalous Results between Dilatometry and Thermocouple Measurements*

A typical thermal analysis plot is shown in Figure 6. Samples were heated in both the CF and FB. Heating rates in CF and FB are 18 and 132 K/min, respectively. The recrystallization peak is noted in both cases. The start and end temperatures of recrystallization for samples heated in FB and CF are listed in Table IV.

Thermal analysis results show that temperatures at the start and end of recrystallization decrease with increasing heating rate. This is in contrast to the results obtained by both dilatometry and DSC experiments, which showed a higher recrystallization temperature at high heating rates. In general, low heating rate results in greater recovery, and hence lower driving force for

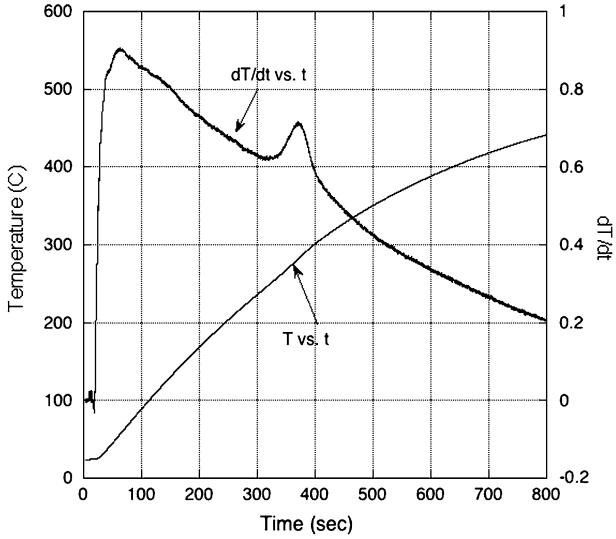

Fig. 6—Thermal analysis of A356 alloy during heating in CF.

Table IV. Recrystallization Data of As-Cast A356 Alloy from Thermal Analysis Experiments

Furnace	Heating Rate (K/min)	Recrystallization Start Temperature [K (°C)]	Recrystallization End Temperature [K (°C)]
FB	132	447 (174)	566 (293)
CF	18	526 (253)	584 (311)

recrystallization (or higher recrystallization temperature). It may be worthwhile to mention that thermal analysis was conducted on the as-cast alloy (without machining), whereas both dilatometric and DSC experiments were conducted on machined samples. In addition, dilatometric and DSC experiments were conducted on very small samples with relatively high surface area per unit volume as compared to samples on which thermal analysis tests were conducted. It is well known that surface energy per unit volume contributes to the driving force for recrystallization and enhances recrystallization kinetics. However, further study is needed to understand the role of machining and surface area per unit volume on recrystallization kinetics.

D. *Microstructural Observations*

1. *SEM analysis*

Typical as-cast microstructures of A356 alloy are shown in Figures 7(a) and (b); they consist of primary α-Al dendrites, eutectic Al, and eutectic Si particles. In addition, some other phases such as Mg_2Si- and Fe-rich intermetallics are also observed. Eutectic Si phase exhibits fibrous morphology, which is typical in Sr-modified as-cast Al-Si alloys. On solution heat treating, the eutectic Si undergoes spherodization and the Al near the eutectic Si particles undergoes

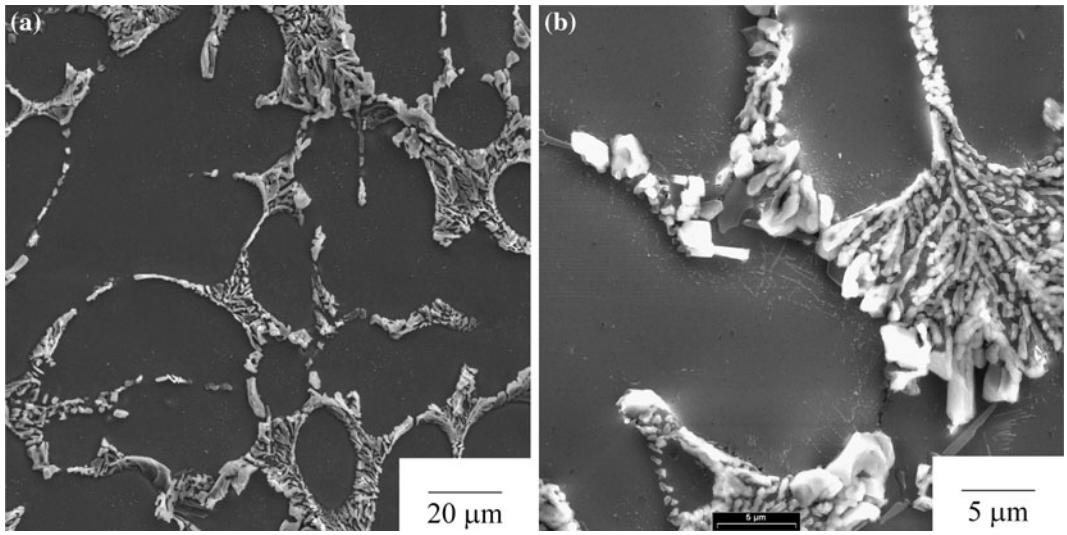

Fig. 7—Typical as-cast SEM microstructure of Al-Si-Mg alloy: (*a*) dendritic structure and (*b*) eutectic Si.

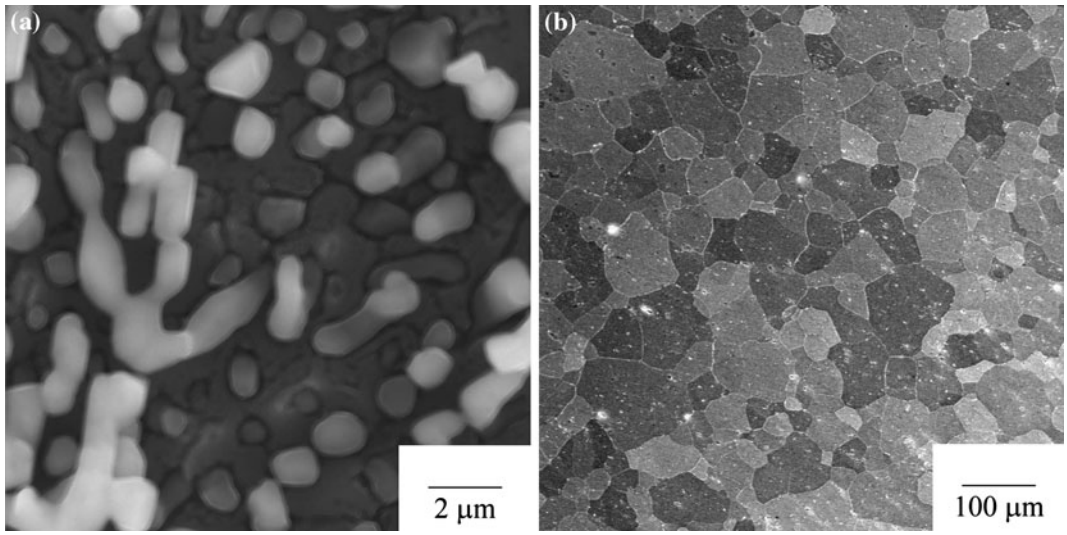

Fig. 8—Typical SEM images showing (*a*) preferential recrystallization of eutectic Al grains in Al-Si-Mg cast alloy near Si phase and (*b*) uniform recrystallization of primary Al grains in Al-Mg-Si (7075) wrought alloy.

recrystallization, as shown in Figure 8(a). It is clearly observed that recrystallization is limited to the eutectic region and at the periphery of primary dendrites (close to eutectic Si). No recrystallized grain is observed at the center of primary Al dendrites. The Al/Si interface is the heterogeneous site for nucleation of recrystallized grains, since all recrystallized grains have a common boundary with Si phase. Recrystallization of eutectic grains was detected during dilatometry, DSC, and the thermal analysis test. For comparison purposes, a typical recyrstallized microstructure of wrought Al-Mg-Si alloy (7075) is shown in Figure 8(b). It shows uniform recrystallization of primary Al grains as opposed to the preferential recrystallization in the as-cast Al-Si-Mg alloy (shown in Figure 8(a)).

Recrystallization in cast alloys is confined to regions near Si particles, because thermal stress is high near the Si/Al interface. The size of the elasto-plastic deformation zone (Z), which is the region stressed due to thermal mismatch, can be estimated by[21]

$$Z = r\left[\frac{(\alpha_m - \alpha_p)\Delta T_o E_m}{(1 - \nu_m)\sigma_y}\right]^{\frac{1}{3}} \quad [2]$$

where r = radius of Si particle, α_m = coefficient of thermal expansion of Al matrix (22.7 μm/m K[22]), α_p = coefficient of thermal expansion of Si particle (2.6 μm/m K[22]), ΔT_o = temperature difference, E_m = Young's modulus of Al matrix (70 GPa[22]), ν_m = Poisson's ratio of matrix (0.34[22]), and σ_y = yield strength (96.53 MPa[10]). In the preceding equation, the following assumptions were made:[21]

(1) particle is spherical and isolated in the matrix,
(2) particle/matrix interface is stable (no dissolution or spherodization),

(3) particle is elastic, and
(4) alloy contains monosize particles.

It is reasonable to assume that below the recrystallization temperature, the interface is stable and no morphological transformation of Si takes place. The calculated value of the elasto-plastic zone size is plotted in Figure 9 as a function of Si particle size for different values of temperature differences (ΔT). The elasto-plastic zone size is of the same order as the particle size and increases with increasing temperature difference. The matrix is stressed in the elasto-plastic zone; hence, it is reasonable to expect that recrystallization should occur in this region. The microstructural observation of elasto-plastic zone size is consistent with the calculated value. The size of recrystallized grain is of the same order as that of the Si particle. The preceding model explains why recrystallization in as-cast Al-Si alloy is confined to regions near the eutectic Si, and the reason for smaller recrystallized grains compared to those commonly observed in wrought Al alloys.

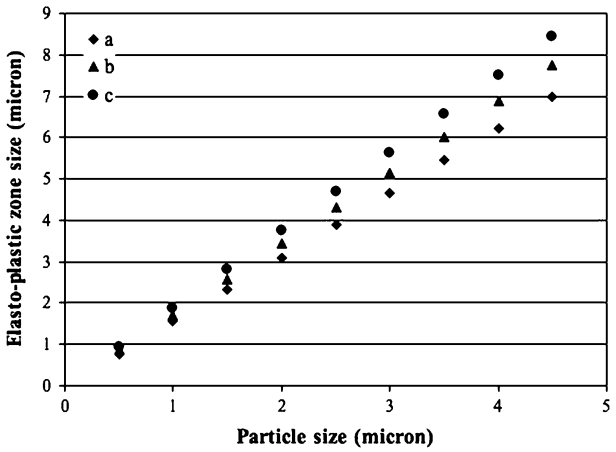

Fig. 9—Effect of particle size and temperature on elasto-plastic zone size in Al-Si alloy: (*a*) ΔT = 170 K (170 °C), (*b*) ΔT = 230 K (230 °C), and (*c*) ΔT = 300 K (300 °C).

2. *TEM analysis*

TEM samples were prepared at various microstructural locations to study the effect of the heating rate during the heating stage of solution heat treatment. Figures 10(a) and (b) show typical TEM micrographs of A356 cast alloy in (a) a specimen heated to 813 K (540 °C) in a FB at 132 K/min and in (b) a specimen isothermally held at 813 K (540 °C) in FB for 30 minutes. In a previous study,[8] it was noted that it takes 4 minutes to heat the sample to 813 K (540 °C) in an FB. The TEM foils were machined from the periphery of the dendrite (including a part of Si). Figure 10(a) reveals that dislocations are generated during the heat-up stage (FB treatment) at the Si/Al interface due to the thermal mismatch between Al and Si particles. There is a difference in the order of magnitude between the coefficient of thermal expansion of Al and Si phases. Due to the high heating rate in FB, thermal stresses generate dislocation networks near the Si/Al interface. The presence of these dislocations indicates that the Si/Al interfaces are subjected to thermal stress, which acts as the driving force for recrystallization of Al grains. No dislocations are observed in the center of the primary dendrite. This indicates that the magnitude of thermal stress decreases away from the Al/Si interface. In addition, it also explains why recrystallized grains were not observed in the center of the dendrites. On isothermal holding the A356 alloy for 30 minutes, a significant annihilation of dislocations was noted. Dislocation networks generated during the temperature ramp-up stage grow and are annihilated during isothermal holding, thus decreasing the overall dislocation density.

On the contrary, no dislocations are observed near the Si/Al interface when the casting was heated at a slow heating rate (18 K/min) in the CF (Figure 11(a)). The sample was heated slowly in the CF for 30 minutes and subsequently taken out of the furnace and cooled in still air. As expected, isothermal holding of the casting at 813 K (540 °C) in a CF for 6 hours does not reveal any structural features such as dislocations near the eutectic Si/Al interfaces (as shown in Figure 11(b)). The absence of dislocations in samples heated in the CF (slow heating rate) indicates that lower thermal stresses are generated. Thus, it is clear that a high heating rate

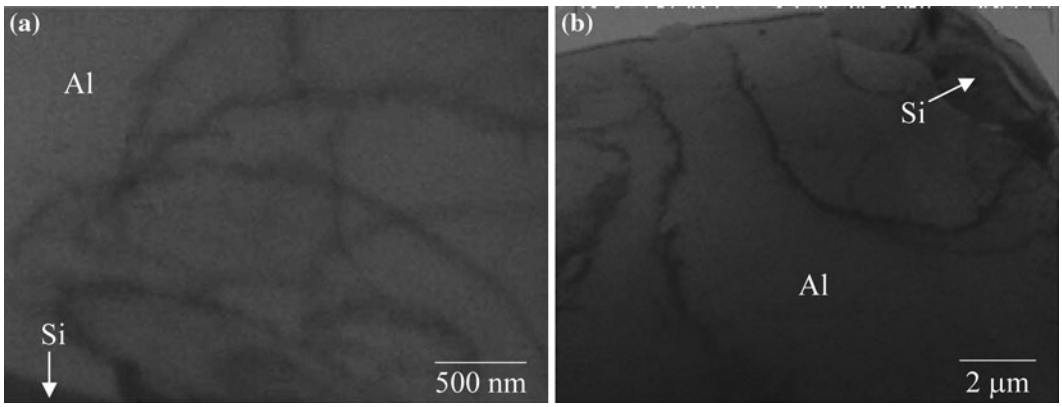

Fig. 10—TEM micrograph showing dislocation near Si/Al interface in Al-Si-Mg alloy heated to 813 K (540 °C) using FB in (*a*) 4 min (magnification = 27,000 times) and (*b*) isothermally held at 813 K (540 °C) for 30 min (magnification = 14,000 times).

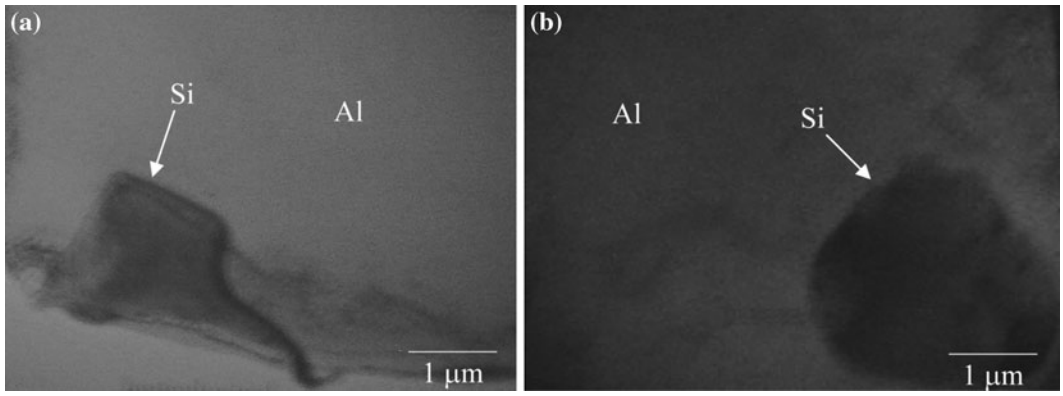

Fig. 11—TEM micrograph of A356 alloy heated to 813 K (540 °C) in (*a*) 30 min (using a CF) and (*b*) isothermally held at 813 K (540 °C) for 360 min (magnification = 27,000 times).

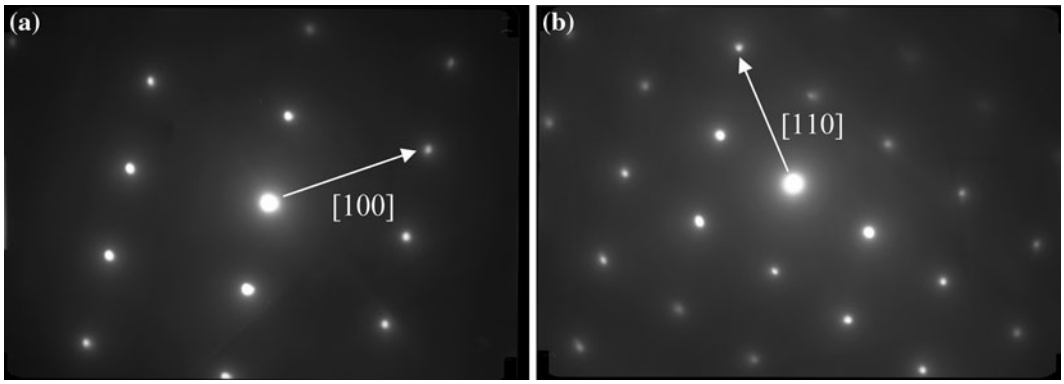

Fig. 12—SAED pattern of (*a*) Al and (*b*) Si (camera length = 100 cm).

results in generation of greater thermal stresses at the particle/matrix interface. The selected area electron diffraction (SAED) patterns of Al and Si are shown in Figures 12(a) and (b), respectively.

E. *Fundamental Difference between Recrystallization in As-Cast vs Wrought Al Alloys*

The driving force for recrystallization in as-cast Al-Si-Mg (A356) alloys is due to the thermal stresses generated at the Al/Si interface owing to the thermal mismatch between Al and Si particles. The coefficient of thermal expansion of Si (2.6 μm/m K) particles is lower than that in Al (22.7 μm/m K).[22] Thermal stresses induce thermal strains in the Al matrix. The amount of thermal stress generated at the Si particle/Al interface due to thermal mismatch at annealing temperatures can be estimated.[23]

Assuming a single spherical elastic particle in an elastic matrix, Brooksbank and Andrews[23] reported that the maximal shear stress, τ_M, that acts in planes oriented at 45 deg with respect to the radial vector of the sphere is given by

$$\tau_M = \frac{3}{2}\frac{(\alpha_2 - \alpha_1)(T_a - T_f)R^3}{\left[\frac{(1+\nu_2)}{E_2} + \frac{2(1-2\nu_1)}{E_1}\right] r^3} \qquad [3]$$

where indices 1 and 2 refer to the particle and matrix, respectively, and $(T_a - T_f)$ = temperature difference from stress-free state, α = mean coefficient of thermal expansion over $(T_a - T_f)$ range, E = Young's modulus, ν = Poisson's ratio, R = radius of particle, and r = distance from the center of the inclusion.

For the case of the Al-Si system, by taking $\alpha_1 = 2.6 \times 10^{-6}$/K and $\alpha_2 = 22.7 \times 10^{-6}$/K, $E_1 = 165$ GPa, $E_2 = 70$ GPa, $\nu_1 = 0.22$, $\nu_2 = 0.34$, $(T_a - T_f) = 20$ K (20 °C), and dimensional factor $(R/r) = 1$[22] in Eq. [3], the maximal shear stress at the interface that would be induced by a temperature change of 20 K (20 °C) equals 23 MPa. The lowest temperature at which recrystallization took place was 470 K (197 °C). Substituting $T_f = 470$ K (197 °C) and $T_a = 300$ K (27 °C) (room temperature) in Eq. [3], and keeping values of all other parameters at the values given previously, the evaluated value of the maximal shear stress is 198 MPa. This shows that significant thermal stress can be generated at the particle/matrix interface for recrystallization of Al. However, the model is a rough approximation, since it is based on the assumption that the Si particle is spherical and the dimensional factor (R/r) in Eq. [3] is assumed to be unity. It is a fact that there is more than one Si particle in the Al matrix, and Si particles are not always spherical. Hence, the dimensional factor (R/r) in Eq. [3] can be lower than unity, and consequently, the maximal shear stress will be higher than the estimated value. The value obtained by the preceding model is a conservative number. Local plasticity occurs in the vicinity of the particle/matrix interface during solution

heat treatment[23] due to high thermal stresses. In general, local plasticity owing to thermal mismatch results in high dislocations in the Al matrix, which is well known to enhance recrystallization kinetics.

Since the thermal stress is highest at the particle/matrix interface, it is more likely that the interface will act as the nucleation site for recrystallization. Thermal stresses significantly reduce away from the particle/matrix interface. This is evident from the dislocation pileup at the Si/Al interfaces (as shown in Figure 10(a)) and the lack of it thereof at locations farther away from the interface. The absence of dislocations at locations farther away from the interface indicates that the matrix at the center of the dendrite experiences reduced thermal stresses. Hence, the driving force for recrystallization at the center of the dendrite is too low for recrystallization to occur. Consequently, no recrystallization was observed at the center of dendritic regions. The differential nature of thermal stress in the Al matrix of as-cast Al-Si alloys causes recrystallization to be a localized phenomenon confined mainly near the vicinity of Si particles. On the contrary, recrystallization in wrought alloys takes place uniformly throughout the Al matrix. Typical recrystallized grains observed in the Al 7075 wrought alloy are shown in Figure 8(b). In the latter, the stored mechanical energy due to cold working is the driving force for recrystallization. Since the stored mechanical energy is uniform throughout the matrix, recrystallization takes place uniformly. In addition, owing to the differences in driving force for recrystallization, cast alloys and wrought alloys exhibit completely different recrystallization behaviors. In the case of wrought alloys, recrystallization can be completed by one annealing treatment, whereas in the case of cast alloys, even during the reheating cycle, recrystallization is observed. This is evident from the reappearance of the recrystallized peak in the dilatometry plot, where the sample was reheated (*i.e.*, second thermal cycle), as shown in Figure 4 and Table III. Whereas in wrought Al alloys, stored mechanical energy is consumed during one recrystallization process. Moreover, in cast alloys, the heating cycle is accompanied by a rapid cooling cycle, during which thermal stresses are regenerated at the Al/Si interfaces providing the driving force for recrystallization (heating and cooling).

Fundamental differences between recrystallization in as-cast and wrought alloys are summarized in Table V. These differences in recrystallization behavior arise due to differences in driving forces. Recrystallization is known to play a significant role in wrought alloys to increase ductility. However, the role of recrystallization in cast alloys is not well studied. One technical difficulty to study the role of recrystallization in cast alloys is to decouple its effect from other microstructural changes occurring during the solution heat-treatment process. Typical examples of microstructural changes during solution heat treatment are as follows: spherodization of Si and intermetallic phases, dissolution of intermetallic phases, reduction of microsegregation, and localized recrystallization of the Al matrix. These microstructural changes have a compounded effect on the final mechanical properties of the material. Some possible effects that might result owing to recrystallization in as-cast Al-Si-Mg alloys are as follows: (1) formation of precipitate-free zone or grain boundary precipitates; and (2) formation of soft zone in the Al matrix, thus providing an easy path for crack propagation during tensile or fatigue testing.

Table V. Differences Between Recrystallization Cast Al-Si and Wrought Al Alloy

Cast Alloy	Wrought Alloy
Driving force: thermal stress ($\Delta\alpha$)—*in situ*	driving force: stored mechanical energy—*ex situ*
Localized phenomenon, near Si particles	uniform throughout the Al matrix
Nucleating site: particle/matrix interface	nucleating sites: dislocation, point defect, grain boundary
Two types of boundaries: Al/Al, and Al/Si	one type of boundary: Al/Al

IV. CONCLUSIONS

The following critical conclusions are drawn from this study.

1. Due to rapid heating in an FB, dislocations are generated at the Si/Al interface, whereas in a CF, with relatively slow heating rate, no dislocations are observed at the eutectic Si/Al interface.
2. Recrystallization occurs during the temperature ramp-up stage of solution heat treatment in cast A356 alloy. The evaluated value of activation energy of recrystallization in cast A356 alloy is 127 KJ/mol.
3. Recrystallization in cast Al-Si alloys is a localized phenomenon and occurs in the vicinity of eutectic Si particles. This is in contrast to recrystallization in wrought alloys, where recrystallized grains evolve throughout the matrix. The difference between recrystallization behavior in cast and wrought alloys is due to their differences in driving force for recrystallization. In the case of cast Al-Si alloy, the driving force for recrystallization is due to thermal mismatch between Al and Si, which is *in situ* (*i.e.*, generated during thermal cycle), whereas in the case of wrought Al alloys, the stored mechanical energy is the driving force for recrystallization, which is *ex situ* (*i.e.*, generated during cold working prior to thermal treatment).
4. Both dilatometry and DSC tests show that the recrystallization temperature increases with increasing heating rate. This is in contrast to the thermal analysis conducted by temperature measurement. This anomaly, however, is less clearly understood and further investigation is needed to explain the observed result.
5. Creep occurred in the A356 alloy when the sample was heated slowly at a rate of 4.3 K/min. However, samples heated at higher heating rates (520, 130, and 17.3 K/min) did not result in permanent deformation due to creep.

ACKNOWLEDGMENTS

Research sponsored by the Assistant Secretary for Energy Efficiency and Renewable Energy, Office of Freedom CAR and Vehicle Technologies, as part of the High Temperature Materials Laboratory User Program, Oak Ridge National Laboratory, managed by UT–Battelle, LLC, for the United States Department of Energy, under Contract No. DE-AC05-00OR22725. The support from corporate members of the Advanced Casting Research Center of the Metal Processing Institute at WPI is deeply appreciated.

REFERENCES

1. R.E. Sanders, Jr.: *J. Met*., 2001, vol. 53 (2), pp. 21–25.
2. M.N. Becker: *J. Met*., 1999, vol. 51 (11), pp. 26–38.
3. *ASM Handbook*, vol. 2, *Properties and Selection: Nonferrous Alloys and Special-Purpose Materials*, ASM INTERNATIONAL, Materials Park, OH, 1991, pp. 159–61.
4. L. Pedersen and L. Arnberg: *Metall. Mater. Trans. A*, 2001, vol. 32A, pp. 525–32.
5. S. Shivkumar, S. Ricci, B. Steenhoff, D. Apelian, and G. Sigworth: *AFS Trans*., 1989, vols. 89–138, pp. 791–810.
6. M.H. Mulazimoglu, A. Zaluska, F. Paray, and J.E. Gruzleski: *Metall. Mater. Trans. A*, 1997, vol. 28A, pp. 1289–95.
7. P.N. Crepeau: *AFS Trans*., 1996, vol. 103, pp. 361–66.
8. S.K. Chaudhury and D. Apelian: *Metall. Mater. Trans. A*, 2006, vol. 37A, pp. 763–78.
9. S.K. Chaudhury and D. Apelian: *J. Mater. Sci*., 2006, vol. 41, pp. 4684–90.
10. S.K. Chaudhury, L. Wang, and D. Apelian: *AFS Trans*., 2004, vol. 112, pp. 1–16.
11. M. Slamova, M. Karlik, M. Cieslar, B. Chalupa, and P. Merle: *Kovove Mater*., 2002, vol. 40 (6), pp. 389–401.
12. M. Slamova, M. Karlik, M. Cieslar, B. Chalupa, and P. Merle: *Kovove Mater*., 2003, vol. 41 (1), pp. 51–62.
13. X. Peng, J. Yang, Y. Chen, and Y. Yin: *Int. J. Solids Struct*., 2003, vol. 40 (26), pp. 7385–97.
14. S. Sarkar, M.A. Wells, and W.J. Poole: *Mater. Sci. Eng. A*, 2006, vol. 421 (1–2), pp. 276–85.
15. C.F. Yeung and W.B. Lee: *J. Mater. Process. Technol*., 1998, vol. 82 (1–3), pp. 102–06.
16. J.S. Venrano, S.M. Bruemmer, L.M. Pawlowski, and I.M. Robertson: *Mater. Sci. Eng. A*, 1997, vol. 238 (1), pp. 101–07.
17. Y.B. Kim, Y.H. Chung, K.K. Cho, and M.C. Shin: *Scripta Mater*., 1997, vol. 36 (1), pp. 111–16.
18. S. Shankar, Y. Riddle, and M.M. Makhlouf: *Metall. Mater. Trans. A*, 2003, vol. 34A, pp. 705–07.
19. H. Kissinger: *Anal. Chem*., 1957, vol. 29, pp. 1702–06.
20. W. Sha: *Metall. Mater. Trans. A*, 2001, vol. 32A, pp. 2903–10.
21. C.S. Park, M.H. Kim, and C. Lee: *J. Mater. Sci*., 2001, vol. 36 (14), pp. 3579–87.
22. X. Zhou, R. Fougeres, and A. Vincent: *J. Phys: III France*, 1992, vol. 2 (11), pp. 2185–2201.
23. D. Brooksbank and K.W. Andrews: *J. Iron Steel Inst*., 1972, vol. 210, pp. 246–55.